Effects of Temperature and Amount of Nitrogen on Phase Transformation in Tungsten Thin Films

A Thesis

Presented to the Faculty of the Graduate School

of Cornell University

in Partial Fulfillment of the Requirements for the Degree of

Master of Science

by Jiayi Cao

May 2024

© 2024 Jiayi Cao

Abstract

Tungsten thin films were deposited in the metastable beta phase, and their stress response to thermal cycling was evaluated in a high-vacuum environment. The stress behavior is analyzed at different stages, and the change from the beta phase to the stable alpha phase is marked by a noticeable rise in tensile stress. Different amounts of nitrogen were added to the films. A thin film with a higher nitrogen content exhibits a greater stress change throughout the thermal cycling process, demonstrating the critical role of nitrogen in influencing phase stability, which is important for building magnetic random-access memories.

Biographical Sketch

Jiayi Cao is from Raleigh, North Carolina. He earned his Bachelor of Science in Mechanical Engineering from North Carolina State University. He is currently advancing his education by pursuing a Master’s degree in Mechanical Engineering at Cornell University. Throughout his graduate studies, Jiayi has relished the chance to connect and collaborate with outstanding individuals. Additionally, his time in Ithaca has deepened his appreciation for the area's stunning landscapes and diverse terrain, making it a cherished aspect of his experience at Cornell.

Acknowledgments

I would like to thank the members of the Baker Group, including Professor Shefford Baker and his Ph.D. student Yue Zhao, for helping me and providing nitrogen concentration calculations and X-ray crystallography data. Moreover, I would like to thank Kevin Roberts and Brian K. Olmstead at the University of Minnesota Nano Center for providing stress-temperature data. This work was performed in part at the Cornell NanoScale Facility, a member of the National Nanotechnology Coordinated Infrastructure (NNCI), which is supported by the National Science Foundation (Grant NNCI-2025233).

Table of Contents

1. Introduction 1
1.1 Background and Motivation 1
1.2 Tungsten crystal structure and key properties 3
1.3 Thin film basics (tungsten thin films) 4
1.4 Thin film Stress 5
1.5 Thermal cycling 7
1.6 The phase transformation in tungsten films 8
1.7 Effect of nitrogen on tungsten phase transformations 10
1.8 Thesis structure 11
1.9 References 12

2. Experiment Methods 16
2.1 Overview 16
2.2 Thin film growth 16
2.3 Film thickness measurements 19
2.4 Stress-temperature measurements 19
2.5 X-ray diffraction measurements 24
2.6 References 27

3. Discussion 28
3.1 Introduction 28
3.2 Converting flow rate to concentration 28
3.3 Substrate-curvature measurements 30
3.4 Results 31
3.5 Discussion 35
3.6 Conclusion 46
3.7 References 47

4. Summary and Future Proposed Research 49

List of Figures

1.1 The unit cell of α tungsten (BCC) 3

1.2 The unit cell of β tungsten (A15) 3

1.3 Different cases of thin film mismatch leading to compressive or tensile in-plane stress.......... 7

1.4 X-ray diffraction results of tungsten thin films with varying amounts of oxygen before and after thermal cycling 10

2.1 Cross-section view of the sputtering chamber in PVD 18

2.2 Working mechanisms of wafer stress measurement.......... 21

2.3 The relationship between the angle and moving distance *x* 22

2.4 Cross-section view of X-ray diffraction under regular condition 26

2.5 Cross-section view of X-ray diffraction to prevent diffraction from the silicon substrate 26

3.1 XRD result of tungsten thin film with an amount of 1.5 sccm nitrogen before thermal cycling 32

3.2 XRD result of tungsten thin film with an amount of 2 sccm nitrogen before thermal cycling 33

3.3 XRD result of tungsten thin film with an amount of 1.5 sccm nitrogen after thermal cycling 33

3.4 XRD result of tungsten thin film with an amount of 2 sccm nitrogen after thermal cycling .. 34

3.5 Stress change of tungsten thin films with different amounts of nitrogen content during thermal cycling.......... 35

3.6 Stress change of tungsten thin films with different amounts of nitrogen content during thermal cycling in 6 different stages 36

3.7 Stress of tungsten thin film with 7.27 at.% of nitrogen at a temperature range between 20 degrees and 400 degrees Celsius.......... 38

3.8 Stress of tungsten thin film with 9.49 at.% of nitrogen at a temperature range between 20 degrees and 400 degrees Celsius.......... 39

3.9 Stress of tungsten thin film with 7.27 at.% of nitrogen at a temperature range between 580 degrees and 820 degrees Celsius.......... 40

3.10 Stress of tungsten thin film with 9.49 at.% of nitrogen at a temperature range between 740 degrees and 820 degrees Celsius 40
3.11 Stress of tungsten thin film with 7.27 at.% of nitrogen during the cooling stage at a temperature range between 700 and 20 degrees Celsius 41
3.12 Stress of tungsten thin film with 9.49 at.% of nitrogen during the cooling stage at a temperature range between 700 and 20 degrees Celsius 42
3.13 Two stress jumps in phase transformation of tungsten thin films 43
3.14 Stress in the tungsten thin films at the start and end 46

Chapter 1

Introduction

1.1 Background and motivation

Tungsten is a rare metal discovered and identified as a new element in 1781 and is noted for having the highest melting point (3,410°C) of all known metal elements [1]. It saw limited use for about a century after which it started being used in high-speed steel, a special mix of steel and tungsten that could maintain its strength at very high temperatures [2]. In 1900, it was presented at the world exhibition in Paris as an exciting new material, and in 1903, tungsten started seeing use in light bulbs because of its high melting point and high electrical conductivity suited for incandescence [3]. Tungsten has two phases, the equilibrium alpha phase and the metastable beta phase. Which one dominates depends on the fabrication method and the system's thermal environment; in either case, upon annealing at sufficiently high temperatures and durations, only the thermodynamically stable alpha phase remains [4].

The equilibrium alpha phase of tungsten is characterized by its high melting point, and strength [5]. It also has high thermal conductivity and a low coefficient of thermal expansion [6]. These properties make it a desirable material in many industrial applications. Currently, alpha tungsten is frequently used in alloyed forms for heating elements and filaments [7].

Many practical applications instead call for the beta variant of tungsten, as it too has unique properties. Hartmann et al. were the first to find beta tungsten in 1931 in dendritic metallic deposits formed on cathodes [8]. It sports a relatively high electrical resistivity, about an order

of magnitude higher than that of its alpha equilibrium phase [9]. The initial fascination with beta tungsten thin films accordingly arose from their remarkable superconducting characteristics at low temperatures [10]. Landmark studies of the superconductivity and associated microstructure, growth, resistivity, and stress in thin films of beta tungsten were performed by Bond et al. in 1965 [11] and by Petroff et al. in 1973 [12].

A significant increase interest in beta tungsten thin films followed reports of the unearthing of their giant spin hall effect by Pai and others in 2012 [13]. This particular property has sparked increased enthusiasm for studying this material's potential applications in magnetic random-access memories due to its giant spin hall effect, which can efficiently convert charge current into spin current [14-16]. They also find uses in X-ray masks and mirrors, field emitters, diffusion barriers in the semiconductor industry, and photonic crystals [17].

Prior studies have shown that oxygen has the ability to stabilize beta tungsten (i.e., raise the temperature required for transformation to its alpha phase) [18]. Indeed, photoemission and X-ray diffraction (XRD) studies have reported the formation of various tungsten oxides, WO_x, as well as interstitial oxygen (zero valence state) embedded in the tungsten films [19-22]. Subsequently, studies where nitrogen was used rather than oxygen have shown a similar effect in stabilizing the beta phase [23], and nitrogen has distinct advantages over oxygen due to the metallic nature of the amorphous nitride [24].

In this study, we focus on tungsten thin films grown on silicon wafers in an argon plasma with a dilute nitrogen content. Our interest is primarily in the metastable beta phase of tungsten, as opposed to its equilibrium alpha phase, due to its many practical uses in various electronic and spintronic applications. During the manufacturing process of magneto-resistive random-access memory, tungsten thin film could experience a high temperature [25]. Because of the high temperature, stress growth in the tungsten thin films during thermal cycling can cause cracking and delamination. Comprehending the impacts of nitrogen and phase transformation on stress development in these films is crucial for preventing mechanical breakdowns in devices.

1.2 Tungsten crystal structure and key properties

The alpha phase of tungsten is a common body-centered cubic (BCC) structure, whereas the beta phase is found in an A15 crystalline structure that is more complex and less common, see Figures 1.1 and 1.2 [26]. At ambient conditions, the two phases tend to coexist in as-deposited films, as most vapor deposition methods are of a non-equilibrium nature. Annealing is the easiest way to convert the metastable beta structure to its stable alpha counterpart.

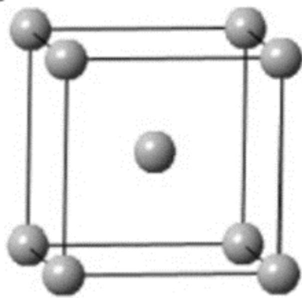

Figure 1.1 The unit cell of α tungsten (BCC).

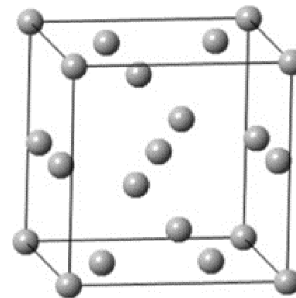

Figure 1.2 The unit cell of β tungsten (A15).

As illustrated in Fig. 1.1, alpha tungsten shares the same basic crystal structure with many other common metals, such as iron, chromium, and molybdenum, where its unit cell holds one atom at each corner and one atom at each center of the cube. The lattice constant of alpha tungsten is 3.165 Å [27]. This body centered cubic structure has a coordination number of 8, meaning that each atom is surrounded by eight nearest neighbors. One important feature of the BCC structure is its relatively low packing density, making it less dense than, e.g., common face-centered cubic and hexagonal close-packed structures. The nature of the BCC structure leads to lower ductility and higher brittleness than the face-centered cubic structure because it is not conducive to facile dislocation propagation.

In Fig. 1.2, the unit cell of beta tungsten is illustrated in its A15 crystal structure, in which one atom is positioned at each corner of the cubic structure with an atom placed at its center and two atoms at each surface. The lattice constant of beta tungsten is 5.05 Å [27]. As mentioned above, this uncommon crystal is particularly well-known for its high-temperature superconducting properties [28].

1.3 Thin film basics (tungsten thin films)

When a film is considerably thinner than the substrate that it's applied to, it's considered a thin film. These films, often ranging from a few hundred nanometers to a few micrometers thick, are applied to substrates using methods such as plasma spraying or physical vapor deposition, or they may be attached to substrates through processes like sintering and diffusion bonding. The continuum mechanics framework proposed for analyzing stress, the curvature of the substrate,

and fracture in such thin films are versatile and relevant to a wide array of practical scenarios, including optical coatings, microelectronics, and magnetic storage devices [29]. The reasons for using thin films vary and may be required due to the small scale of the devices (e.g., microchips), physical requirements (e.g., lens coatings), and even just due to cost restrictions (same functionality but less cost than solid materials or thicker films). In the remainder of this thesis, we are concerned only with systems wherein such thin films are attached to silicon substrates, which are much thicker than the films.

1.4 Thin film stress

Film stresses can typically be classified into two main types. The first type, known as growth stresses, emerges from stress patterns that develop in films during their formation on substrates or adjacent layers. These stresses vary significantly based on the materials used, the temperature of the substrate during deposition, the rate of growth, and the conditions within the growth chamber. Recent advancements in non-destructive techniques for measuring stress in real-time and monitoring the growth surface have enabled the observation of how growth surface characteristics and overall stress levels change during film development. This progress has shed light on the origins of film stress and resulted in further distinguishing between stresses that occur at different stages of the growth process and those that remain after growth has concluded. Growth stresses, which are generally consistent for a specific process and maintain their levels at room temperature well after growth, are also referred to as intrinsic stresses, although this term is somewhat limited in describing the phenomenon.

The second type of film stress, known as extrinsic stress, results from changes in the film's physical environment after it has been formed. These stresses, often related to the film's interaction with a substrate, typically manifest only when the film is attached to a substrate.

The thin film's constrained geometry explains the focus on two stress directions. Since the film is thin relative to its lateral dimensions, the stress across the thickness (out-of-plane) is often uniform and less variable than the stress spreading over the large surface area (in-plane). The mechanical properties and behavior of thin films are predominantly influenced by in-plane stresses. The emphasis on in-plane stress arises from the fact that thin films are typically constrained by the substrate on which they are deposited, limiting the extent of out-of-plane deformation. In contrast, in-plane stress, which acts parallel to the surface of the film, significantly influences the film's mechanical, electrical, and optical properties due to the film's extensive interface with the substrate. In-plane stress in thin films can result from various sources, such as thermal expansion mismatch between the film and the substrate, grain growth during and after deposition, and the intrinsic stress induced by the deposition process itself.

Substrate interaction stresses arise when the film and substrate have different lateral dimensions in a relaxed state but are compelled to have identical dimensions. These stresses always exist in thin films and can reach remarkably high levels, which can complicate numerous thin film applications. Figure 1.3 illustrates the different cases of thin film mismatch leading to compressive or tensile in-plane stress.

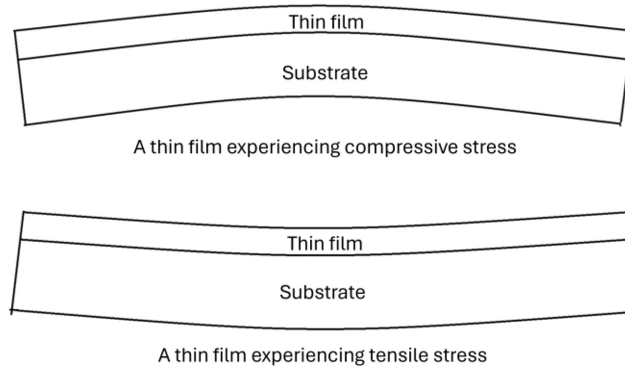

Figure 1.3 Different cases of thin film mismatch leading to compressive or tensile in-plane stress.

1.5 Thermal cycling

If the coefficients of thermal expansion (CTE) of a thin film and its substrate differ, a temperature variation in the film/substrate system will result in altered stress levels within the film. In the situation of a tungsten thin film on a silicon substrate, tungsten has a higher coefficient of thermal expansion (CTE) than silicon. As a result, tungsten thin films will expand or contract faster than the silicon substrate as the temperature is increased or decreased, and the thin film thus experiences strain as it is compelled to take on the in-plane lattice parameters of the thicker substrate. The in-plane strain, $\varepsilon_{thermal}$, can be calculated using the CTE of the film, α_f, and the substrate, α_s, as a function of temperature according to Segmuller [30]: where T is the final temperature, and T_0 is the initial temperature.

$$\varepsilon_{thermal} = -\int_{T_0}^{T} \{\alpha_f(T) - \alpha_s(T)\}\, dT \qquad 1.1$$

The equation 1.1 can be simplified to:

$$\varepsilon_{thermal} = -\big(\alpha_f(T) - \alpha_s(T)\big)(T - T_0) = -\Delta\alpha\Delta T \qquad 1.2$$

where ΔT is the temperature change. The change in stress in the thin film is given by:

$$\Delta\sigma = Y_f\,\varepsilon_{thermal} = \frac{E_f}{1 - \upsilon_f}\varepsilon_{thermal} \qquad 1.3$$

where Y_f is the biaxial elastic modulus of the thin film.

Besides the stress and strain alterations caused by differential thermal expansion, thermal cycling can impact the crystal structure, morphology, and composition in different ways. These changes can influence the resulting stress in a film. Notable effects on film stresses can arise from grain growth, oxidation, and changes in crystal texture or phase at high temperatures.

1.6 The phase transformation in tungsten films

In 2006, Robert Knepper used thermal cycling to explore phase transformations in tantalum thin films [31]. Like in tungsten, tantalum has two phases, a metastable beta phase and a stable alpha phase. Once the metastable beta phase changes to its stable alpha phase, it cannot revert. During this phase transformation, the density of tantalum increases, as the volume of the same amount of matter decreases, and this increase in density causes changes in internal film stress [31]. In the study of tantalum, it was found that adding more oxygen into tantalum thin films requires a higher temperature to finish phase transformation [31].

Similar to tantalum, the metastable phase of tungsten can be stabilized by nitrogen or oxygen [23]. These reports differ on exactly how these gases accomplish the stabilization of the metastable phase of tungsten, and our study is an effort to further the understanding in this regard by studying the stress behavior as a function of temperature.

The transformation from beta to alpha tungsten in thin films has been studied previously with varying results. Because of different deposition conditions and film thickness, the temperature of transformation has been observed to range between 500 and 700 degrees Celsius [32], and, in some situations, the transformation temperature has even reached above 700 degrees Celsius [33].

In prior experiments, researchers have performed phase transformation experiments using different additives. For example, O'Keefe et al. studied the phase transformation of beta tungsten with varying amounts of oxygen under different temperature conditions [32]. In their study, they report X-ray diffraction results only before and after thermal cycling, as shown in Figure 1.4. However, these experiments do not provide any thermomechanical results, including how stress changes during thermal cycling, which is important for practical applications. Our study aims at improving on that by studying the thermal effects on the beta tungsten film stress, and its transformation to the alpha phase during heating.

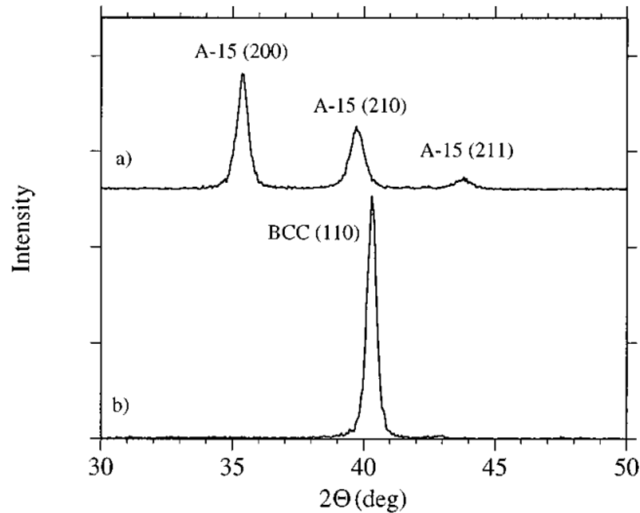

Figure 1.4 X-ray diffraction results of tungsten thin films with varying amounts of oxygen before and after thermal cycling.

This thesis thus focuses on the thermomechanical behavior and microstructure of tungsten thin films. A key interest here is to prevent the phase transformation from the beta to the alpha phase so that the desired properties of the metastable beta phase and the concomitant functionality enabled thereby can be retained. Therefore, it is important to understand the interplay between film preparation, processing, microstructure, and stress.

1.7 Effect of nitrogen on tungsten phase transformations

It has previously been found that adding nitrogen stabilizes the beta phase in tungsten thin films [34]. Nitrogen adsorbates, which promote the nucleation of beta-tungsten more readily than alpha-tungsten, provide the necessary nucleation on the surface of the substrate [23]. Nitrogen adsorbate clusters, which promote the nucleation of beta tungsten, are thought to provide suitable templates for the formation of the tungsten tetrahedra, which pack as edge-sharing tetrahedra to form the icosahedral triangulated coordination polyhedral that form the

crystalline grains of the A15 structure [23]. In Chapter 2, a study similar to the previous one is conducted, albeit with a higher nitrogen concentration. Beyond performing X-ray diffraction analyses, the stress-temperature behavior of the beta tungsten thin film on silicon is examined in detail, observing its response during both heating and cooling cycles between room temperature and 900°C.

1.8 Thesis structure

This thesis is arranged into four chapters. The first chapter provides background information on tungsten thin films, summarizes prior research in this area regarding their structure and thermomechanical properties, and explains the motivation behind the current study. Chapter 2 describes the experimental study performed within the realm of this thesis, and provides details about the setup and parameters, and reports on the findings of the study. Chapter 3 reports the results and findings from our experiment. Chapter 4 is devoted to distilling the key conclusions and a discussion about these in light of the goal of the study and additional studies that are suggested to promote further understanding.

1.9 References

1. Kazantzis, G. (2007). Tungsten. In *Elsevier eBooks* (pp. 871–879). https://doi.org/10.1016/b978-012369413-3/50099-9

2. Chaus, A. S., & Porubski, Y. (2012). Effect of modifying tungsten additions on formation of primary structure of R6M5-type high-speed steel. *Physics of Metals and Metallography*, *113*(11), 1068–1078. https://doi.org/10.1134/s0031918x12110038

3. Carlà, M. (2013). Stefan–Boltzmann law for the tungsten filament of a light bulb: Revisiting the experiment. *American Journal of Physics*, *81*(7), 512–517. https://doi.org/10.1119/1.4802873

4. Karabacak, T., Wang, P.-I., Wang, G.-C., & Lu, T.-M. (2005). Phase transformation of single crystal *β*-tungsten nanorods at elevated temperatures. *Thin Solid Films*, *493*(1–2), 293–296. https://doi.org/10.1016/j.tsf.2005.06.059

5. Greger, M., Čížek, L., & Widomská, M. (2004). Structure and mechanical properties of formed tungsten based materials. *Journal of Materials Processing Technology*, *157–158*, 683–687. https://doi.org/10.1016/j.jmatprotec.2004.07.154

6. Lv, Y., Song, J., Lian, Y., Yu, Y., Liu, X., & Zhuang, Z. (2015). The thermal properties of high purity and fully dense tungsten produced by chemical vapor deposition. *Journal of Nuclear Materials*, *457*, 317–323. https://doi.org/10.1016/j.jnucmat.2014.11.095

7. Šmid, I., Akiba, M., Vieider, G., & Plöchl, L. (1998). Development of tungsten armor and bonding to copper for plasma-interactive components. *Journal of Nuclear Materials*, *258–263*, 160–172. https://doi.org/10.1016/s0022-3115(98)00358-4

8. Hartmann, H., Ebert, F., & Bretschneider, O. (1931b). Elektrolysen in Phosphatschmelzen. I. Die elektrolytische Gewinnung von alpha- und beta-Wolfram. *Zeitschrift Für Anorganische Chemie*, *198*(1), 116–140. https://doi.org/10.1002/zaac.19311980111

9. Desai, P. D., Chu, T. K., James, H. M., & Ho, C. (1984). Electrical resistivity of selected elements. *Journal of Physical and Chemical Reference Data*, *13*(4), 1069–1096. https://doi.org/10.1063/1.555723

10. Basavaiah, S., & Pollack, S. R. (1968). Superconductivity in B-Tungsten films. *Journal of Applied Physics*, *39*(12), 5548–5556. https://doi.org/10.1063/1.1656012

11. Bond, W. L., Cooper, A. S., Andres, K., Hull, G. W., Geballe, T. H., & Matthias, B. T. (1965b). Superconductivity in Films of β-Tungsten and Other Transition Metals. *Physical Review Letters*, *15*(6), 260–261. https://doi.org/10.1103/physrevlett.15.260

12. Petroff, P., Sheng, T. T., Sinha, A. K., Rozgonyi, G. A., & Alexander, F. B. (1973). Microstructure, growth, resistivity, and stresses in thin tungsten films deposited by RF Sputtering. *Journal of Applied Physics*, *44*(6), 2545–2554. https://doi.org/10.1063/1.1662611

13. Pai, C., Liu, L., Li, Y., Tseng, H., Ralph, D., & Buhrman, R. A. (2012). Spin transfer torque devices utilizing the giant spin Hall effect of tungsten. Applied Physics Letters, 101(12), 122404. https://doi.org/10.1063/1.4753947

14. Hao, Q., Chen, W., & Xiao, G. (2015). Beta (*β*) tungsten thin films: Structure, electron transport, and giant spin hall effect. *Applied Physics Letters*, *106*(18). https://doi.org/10.1063/1.4919867

15. Sethu, K. V., Ghosh, S., Couet, S., Swerts, J., Sorée, B., De Boeck, J., Kar, G. S., & Garello, K. (2021). Optimization of Tungsten β -Phase Window for Spin-Orbit-Torque Magnetic Random-Access Memory. *Physical Review Applied*, *16*(6). https://doi.org/10.1103/physrevapplied.16.064009

16. Chen, S., Wang, J., Wu, R., Wang, Z., Li, Y., Lu, Y., Zhou, W., Hu, P., & Li, H. (2021). Insights into the nucleation, grain growth and phase transformation behaviours of sputtered metastable β-W films. *Journal of Materials Science & Technology*, *90*, 66–75. https://doi.org/10.1016/j.jmst.2021.02.027

17. Karabacak, T., Wang, P.-I., Wang, G.-C., & Lu, T.-M. (2005). Phase transformation of single crystal *β*-tungsten nanorods at elevated temperatures. *Thin Solid Films*, *493*(1–2), 293–296. https://doi.org/10.1016/j.tsf.2005.06.059

18. Shen, Y., & Mai, Y. (2000). Influences of oxygen on the formation and stability of A15 β-W thin films. *Materials Science and Engineering: A*, *284*(1–2), 176–183. https://doi.org/10.1016/s0921-5093(00)00745-0

19. Petroff, P., Sheng, T. T., Sinha, A. K., Rozgonyi, G. A., & Alexander, F. B. (1973). Microstructure, growth, resistivity, and stresses in thin tungsten films deposited by RF Sputtering. *Journal of Applied Physics*, *44*(6), 2545–2554. https://doi.org/10.1063/1.1662611

20. Gunnar Hägg, & Nils Schönberg. (1954). `β-Tungsten’ as a tungsten oxide. *Acta Crystallographica /*, *7*(4), 351–352. https://doi.org/10.1107/s0365110x54000989

21. Sinha, A. K. (1972). Topologically close-packed structures of transition metal alloys. *Progress in Materials Science*, *15*(2), 81–185. https://doi.org/10.1016/0079-6425(72)90002-3

22. An, V. (2006). Features of β-α transformation in electroexplosive tungsten nanopowders. *Proceedings. The 9th Russian-Korean International Symposium on Science and Technology, 2005. KORUS 2005.* https://doi.org/10.1109/korus.2005.1507657

23. Liu, J., & Barmak, K. (2016). Topologically close-packed phases: Deposition and formation mechanism of metastable β-W in thin films. *Acta Materialia*, *104*, 223–227. https://doi.org/10.1016/j.actamat.2015.11.049

24. Gómez, J., & Haberkorn, N. (2023). Impact of nitrogen impurities on the tungsten properties for application in spintronic. *Applied Physics A*, *129*(6). https://doi.org/10.1007/s00339-023-06695-x

25. Ohshima, N., Shimura, K., Miura, S., Suzuki, T., Nebashi, R., & Hada, H. (2008). Magnetic properties and writing characteristics of magnetic clad lines in magnetoresistive random access memory devices. *Japanese Journal of Applied Physics*, *47*(5R), 3456. https://doi.org/10.1143/jjap.47.3456

26. Murugan, K., Chandrasekhar, S., & Joardar, J. (2011). Nanostructured α/β-tungsten by reduction of WO3 under microwave plasma. *International Journal of Refractory Metals & Hard Materials*, *29*(1), 128–133. https://doi.org/10.1016/j.ijrmhm.2010.09.005

27. Karabacak, T., Wang, P., Wang, G., & Lu, T. (2005). Phase transformation of single crystal β-tungsten nanorods at elevated temperatures. *Thin Solid Films*, *493*(1–2), 293–296. https://doi.org/10.1016/j.tsf.2005.06.059

28. Stewart, G. R. (2015). Superconductivity in the A15 structure. *Physica C-superconductivity and Its Applications*, *514*, 28-35. https://doi.org/10.1016/j.physc.2015.02.013

29. Vinci, R. P., & Vlassak, J. J. (1996). Mechanical behavior of thin films. *Annual Review of Materials Science*, *26*(1), 431–462. https://doi.org/10.1146/annurev.ms.26.080196.002243

30. Segmüller, A., & Murakami, M. (1988). X-ray diffraction analysis of strains and stresses in thin films. In *Treatise on materials science and technology* (pp. 143–200). https://doi.org/10.1016/b978-0-12-341827-2.50010-8

31. Knepper, R., Stevens, B. L., & Baker, S. P. (2006c). Effect of oxygen on the thermomechanical behavior of tantalum thin films during the β–α phase transformation. *Journal of Applied Physics*, *100*(12). https://doi.org/10.1063/1.2388742

32. O'Keefe, M. J., & Grant, J. T. (1996). Phase transformation of sputter deposited tungsten thin films with A-15 structure. *Journal of Applied Physics*, *79*(12), 9134–9141. https://doi.org/10.1063/1.362584

33. Karabacak, T., Wang, P.-I., Wang, G.-C., & Lu, T.-M. (2005). Phase transformation of single crystal β-tungsten nanorods at elevated temperatures. *Thin Solid Films*, *493*(1–2), 293–296. https://doi.org/10.1016/j.tsf.2005.06.059

34. Singh, H., Gupta, M., Gupta, P., Penacchio, R. F., Morelhao, S. L., & Kumar, H. (2023). Role of nitrogen partial pressure, deposition rate and annealing on stability of β-W phase. Applied Physics A, 129(5). https://doi.org/10.1007/s00339-023-06552-x

Chapter 2

Experiment Methods

2.1 Overview

This chapter provides information about the experimental methods used in this thesis. It includes a detailed description of the sputter deposition, stress measurement, and thickness measurement used in this project. Additionally, it also contains an in-depth examination of the measurement methods employed to track phase transformations, such as curvature measurements and X-ray diffraction.

2.2 Thin film growth

Physical vapor deposition (PVD) is a method that utilizes physical mechanisms, including evaporation, sublimation, or ion bombardment of a target, to transport atoms from a solid or liquid source to a substrate. The two primary techniques of PVD, evaporation and sputtering, are commonly employed for film deposition. In this project, sputtering is used for fabrication.

Sputtering constitutes a process wherein the atoms constituting the film on a substrate are procured through the targeted bombardment by energetic ions present within a partially ionized rare gas plasma that includes ionized gas containing an equal number of positive ions and negative electrons. The generation of these ions occurs within the chamber by applying high voltage between electrodes under conditions of low pressure. Ions emanating from the rare gas discharge facilitate the ejection, or sputtering, of atoms from the target material. The characteristics of the films produced via this process are influenced by several factors, including

the choice of gas, the material of the target, the magnitude of power applied, the pressure of the gas, and the geometric configuration of the system.

Sputtering can be performed using methods such as bias, magnetron, radio frequency (RF), or DC sputtering, and, in this project, DC sputtering is used. A DC sputtering consists of two electrodes, which are cathode and anode placed in the vacuum chamber. In this sputtering technique, a negative voltage is applied to the cathode (target material) since it is connected to the negative side of the direct current power supply, and a positive voltage is applied to the anode(substrate). As a high electric potential is applied across the electrodes, the gas becomes a plasma, and the target material bombarded by the highly energetic gas plasma particles thus ejects microscopic particles that then coat the substrate leading to the growth of a thin film thereupon. The cross-section view inside of the chamber is shown in Figure 2.1.

The following are the main steps in the physical vapor deposition (PVD) sputtering process:

1. Vacuum Chamber: Before deposition, the entire chamber is evacuated to a low pressure (2×10^{-7} torr) to prevent contamination during deposition.
2. Gas Introduction: An inert gas, such as argon (Ar), is introduced into the chamber at one end with a total flow rate of 30 standard cubic centimeters per minute (sccm) and exhausted at the other to ensure an appropriate amount of gas is present during the ensuing ionization process.
3. Plasma Generation: A high voltage is applied between the Si wafer attached to the anode and the sputtering target (tungsten) attached to the cathode, which is connected

to the chamber as an electrical ground. Because of the potential difference, a strong electric field is formed inside the gas-filled chamber, causing it to ionize and form plasma.

4. Ion Bombardment and Sputtering: During the sputtering process with a DC power of 400 watts and operating pressure of 3 mTorr, the wafer is placed at the top at a positive potential, while the sputtering gun is placed at the bottom at a negative potential. The positively charged ions in the plasma are accelerated to the target because of the potential difference. During this process, the target material is knocked off by the argon gas ions.
5. Film Deposition: After the target atoms are ablated from the target at the cathode by heavy argon ions, they are attracted to the substrate affixed to the anode and thus deposit onto the substrate surface creating a film of the sputtering target material. The deposition rate is 0.2 nanometers per second, and the deposition time is 1000 seconds.

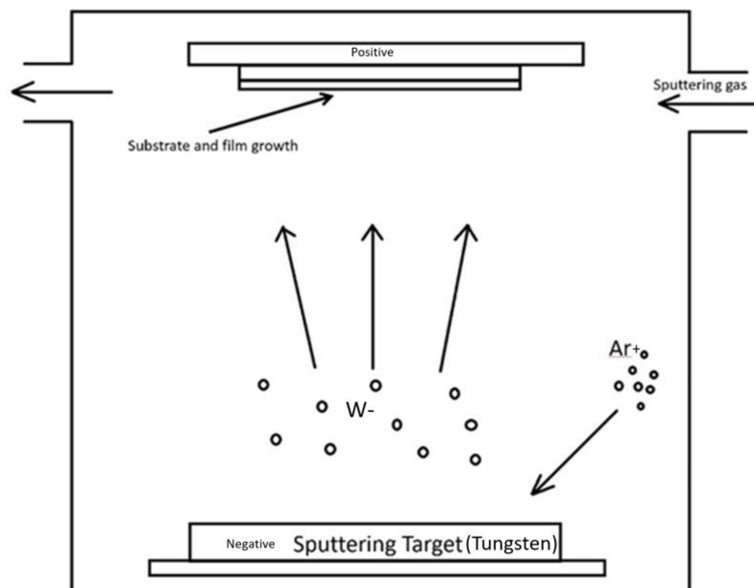

Figure 2.1 Cross-section view of the sputtering chamber in PVD.

2.3 Film thickness measurements

Contact profilometry was used to measure the thickness of deposited films, and it utilized a diamond tip stylus that was moved laterally across a thickness step change in the sample. The height position of the diamond tip measured the surface variations of the sample. Film thicknesses were determined from an average of several scans across the same nominal region.

These witness samples were used to calibrate the precise thicknesses. These are made of about a 1 cm^2 silicon chip coated with a positive photoresist, which is a layer of patterned coating acting as a mask on the surface of a silicon chip. Before the deposition, the photoresist is already patterned on the silicon chip. During the deposition, the tungsten thin film is deposited on the photoresist and silicon chip. After the deposition process, the photoresist is eliminated by immersing the chip in acetone within a beaker deep into an ultrasonic cleaner for 15 minutes. Once the photoresist is removed, the tungsten thin film on the photoresist and photoresist are removed by acetone. Then, the pattern of the tungsten thin film on the silicon chip can be used for step height measurements by using a Dektak profilometer with a scanning length of 400 micrometers. The scanning speed in this study was 20 micrometers/second, and the tip force was 50 mN. All the thin films were found to be about 200 nm thick.

2.4 Stress-temperature measurements

The reported densities of the beta and alpha phases of tungsten are 19.12 g/cm^3 and 19.27 g/cm^3, respectively [1]. Since the mass of the film remains constant during a phase transformation, the only way that the density can increase is by the volume decreasing. Since

the thin film is constrained to the substrate, it therefore experiences tensile stress as the volume decreases. During the thermal cycling process, because of the difference between the coefficients of thermal expansion of silicon and tungsten and density change during the thermal cycling, stress is created inside the tungsten thin films during the heating and cooling. To track the change of the associated thin film stress in real-time during thermal cycling, a substrate-curvature method is employed where the measured curvatures are converted to stresses, which the film experiences during the cycling.

To accurately calculate the change in curvature of a thin film during thermal treatment, a laser scanning method is used. In this method, as the laser scans the film surface, the reflected light beam changes angles as the film curves as a result of the imposed mismatch strain. A position-sensitive photodetector detects these changes, as both the laser and the photodetectors traverse the substrate on a track-mounted moving cart. As shown in Figure 2.2, the curvature of a thin film is calculated from the change of reflected angle divided by the change of moving distance from one end to another end as the photodetector moves.

Thin film stress is calculated by measuring the change in the radius of the curvature of a substrate caused by the deposition of a thin film onto it. To establish a baseline, a reference measurement of the deflection of the bare substrate is first made. Next, the tungsten film is deposited, and that measurement is repeated. Following that, the system is exposed to increasingly higher temperatures, and the stress is calculated based on the curvature every 10 degrees Celsius. The residual stress can be either tensile or compressive – if the atoms in the

tungsten film are on average farther apart than normal, the film experiences compressive stress. Conversely, thin films can experience tensile stress if the atoms are forced closer together than they would be without being attached to the substrate.

Frontier Semiconductor and Toho Technology are two companies currently providing stress-curvature measurement machines. FSM 500, FSM 900TC-VAC, and Flex-2320 are quite common variants used in the thin film community. All of these can measure stress changes during thermal cycling. In this project, FSM 900TC-VAC is used because it can measure the stress change up to 900 degrees Celsius under a high vacuum.

Figure 2.2 illustrates the working mechanisms of stress measurement [2]. *R* is the radius of the curvature, *h* is the thickness of the substrate, and *t* is the thickness of thin films. Figure 2.3 explains how curvature is measured based on the angle change divided by the moving distance [2].

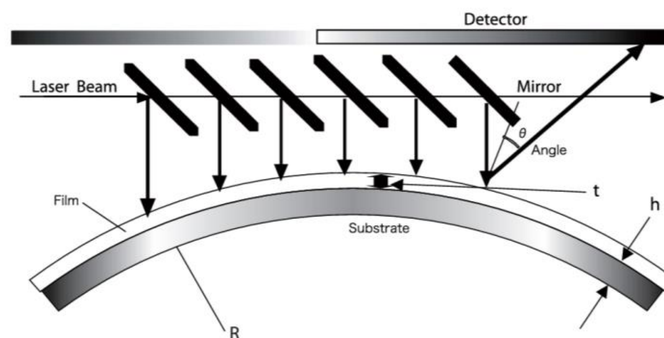

Figure 2.2 Working principle of substrate curvature measurement.

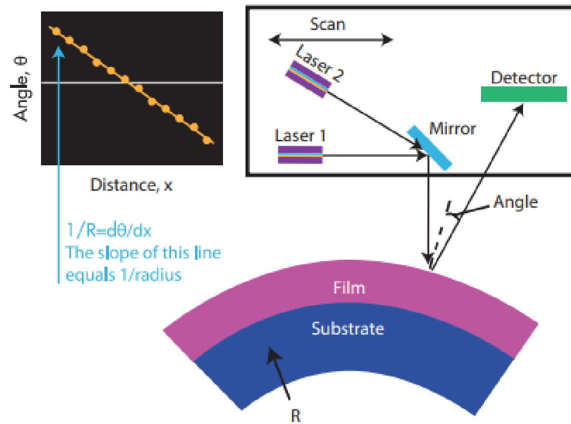

Figure 2.3 The relationship between the angle and moving distance *x.*

When a relatively thin film is deposited onto a substrate, the stress inside thin films can be measured by the substrate's curvature. To quantify the stress from the film curvature, the initial curvature of the bare wafer before film deposition, represented as K_0, is established. Following the deposition of the film, the total curvature of the substrate/film combination, denoted as K_{Tot}, is then measured. The change in curvature due to the film strain is derived from the difference between the two:

$$K_f = K_{Tot} - K_0 \qquad 2.1$$

where the average stress in the film can be found using the Stoney equation (Eq. 2.2) [3]:

$$\sigma_f = \frac{E_s t_s^2}{6(1 - \nu_s) t_f} K_f \qquad 2.2$$

Herein, E_s and ν_s are Young's modulus and Poisson ratio of the substrate, respectively, and t_s and t_f denote the respective substrate and film thickness. The validity of these equations is constrained to situations where the film thickness is considerably smaller than the substrate (as is the case in this study), so the curvature of the thin film varies directly with the curvature of the substrate.

When the film and its substrate undergo heating, they exhibit varying rates of thermal expansion. This disparity arises from the distinct coefficients of thermal expansion between silicon and tungsten, leading to stress development in the tungsten thin films during thermal cycling. Such stress is explained by the film's thermoelastic properties. Equation 2.3 enables the calculation of the rate at which this stress changes.

Upon heating, the film and its substrate expand at divergent rates due to the distinct thermal expansion coefficients of silicon and tungsten. This variance induces stress within the tungsten thin films throughout thermal cycling. The generated stress is characterized by the film's thermoelastic response. The gradient of this stress is quantifiable through Equation 2.3[4], where *Y* represents the biaxial modulus of the film material, and α_s and α_f are the coefficients of the substrate and thin films:

$$\frac{d\sigma}{dT} = Y(T)(\alpha_s(T) - \alpha_f(T)) \qquad 2.3$$

2.5 X-ray diffraction measurements

X-ray diffraction analysis is a facile and common method to determine the crystallographic structure of a material. When a beam of incident X-rays encounters a crystalline structure, it diffracts into a number of specific directions as the electromagnetic waves interact with core electrons in the crystal atoms. As the excited core electrons relax back to their ground levels, additional X-rays are emitted from the affected atoms. These reflected beams interfere constructively or destructively as the distance and angle of the lattice plane change. The measured XRD pattern thus becomes sort of a 'fingerprint' of the crystal structure of the thin film.

These scans mainly aimed to identify the phase(s) of tungsten crystals in a sample and additionally offered insights into the distribution of orientations within these crystal structures. This provided a qualitative assessment of the alignment of crystal planes about the film's surface. The shift of x-ray diffraction peaks from tungsten follows Bragg's law. Peak shifts to lower angles mean a build-up of compressive strain in the film, and peak shifts to higher angles are indicative of tensile stress, as discussed in the next section.

The X-ray diffraction analyses performed on the deposited tungsten thin films in this study relied on a Rigaku SmartLab X-ray diffractometer, which employs a copper radiation source and a scintillator detector to determine the structure of the films. The X-ray equipment was operated at a voltage of 40 kV and a current of 44 mA, with a wavelength of 1.5406 Å.

Bragg's law stipulates that diffraction occurs when the condition $d = \lambda/(2 \times \sin\theta)$ is met and the crystal plane's normal vector aligns parallel to the scattering vector as shown in Figure 2.4. In this equation, *d* represents the spacing between lattice planes, λ refers to the wavelength of the x-rays, and θ is the angle of diffraction. In a two-theta scan, the scattering vector's direction remains constant, while the length of the vector is tuned by changing the angle θ. In this project, the theta/2theta scan was run from 20° to 90° to ensure that all tungsten peaks were captured, as well as to check for any unexpected peaks that would indicate contamination or other compounds, such as tungsten nitrides, oxides, or carbides.

Because the diffraction of silicon in the crystallographic direction is significantly intense—approximately three times the intensity of reflections from beta tungsten—we adjusted the stage by tilting its normal vector two degrees away from the scattering vector. Since the planes are no longer in the Bragg condition, this strategic tilt effectively eliminates reflections from silicon, facilitating unobstructed observations. As shown in Figure 2.5, due to the single-crystalline structure of the silicon substrate in contrast to the polycrystalline structure of tungsten, which exhibits grains oriented in different directions, a precise tilt of two degrees away from the scattering vector enables the observation of diffraction from tungsten thin films without any interference from the silicon substrate.

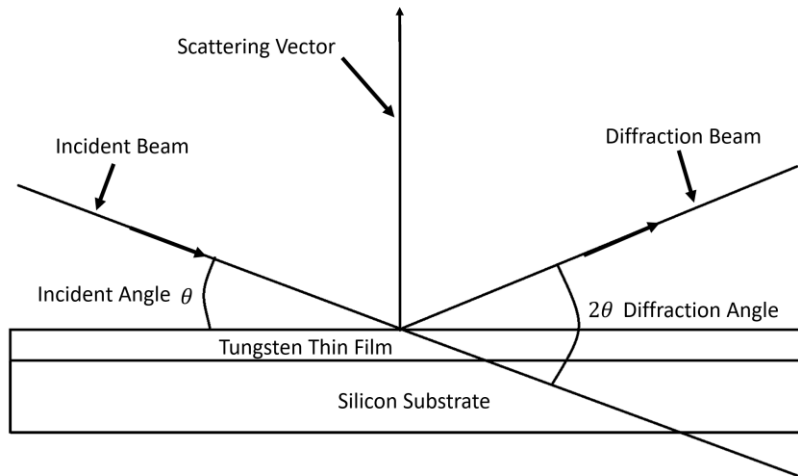

Figure 2.4 Cross-section view of X-ray diffraction under regular conditions.

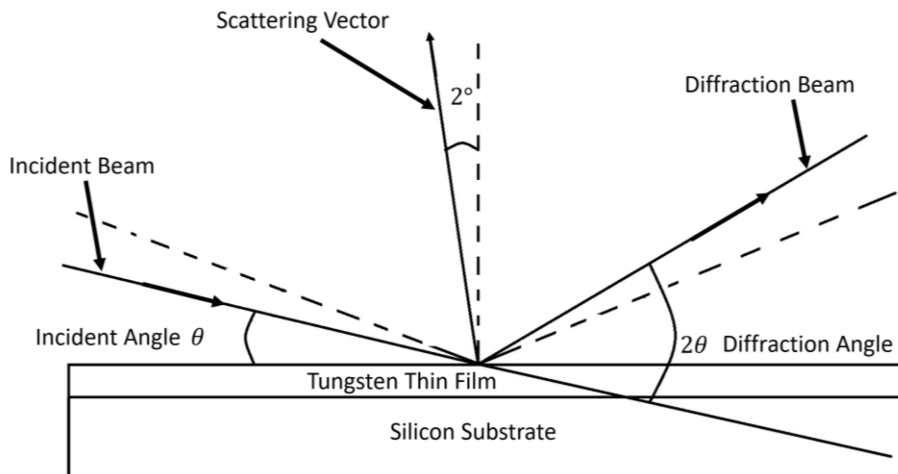

Figure 2.5 Cross-section view of X-ray diffraction to prevent diffraction from the silicon substrate.

2.6 References

1. Nagakubo, A., Lee, H. T., Ogi, H., Moriyama, T., & Ono, T. (2020b). Elastic constants of beta tungsten thin films studied by picosecond ultrasonics and density functional theory. *Applied Physics Letters*, 116(2), 021901. https://doi.org/10.1063/1.5131768

2. Quantum Design Inc. (n.d.). FLX Flexus thin film stress measurement systems TOHO Technology | Quantum Design. https://qd-europe.com/hu/en/product/flx-flexus-thin-film-stress-measurement-systems/

3. Pureza, J. M., Lacerda, M. M., De Oliveira, A. L., Fragalli, J. F., & Zanon, R. A. S. (2009). Enhancing accuracy to Stoney equation. *Applied Surface Science*, 255(12), 6426–6428. https://doi.org/10.1016/j.apsusc.2009.01.097

4. Abadias, G., Chason, E., Kečkéš, J., Sebastiani, M., Thompson, G. B., Barthel, É., Doll, G. L., Murray, C. E., Stoessel, C. H., & Martinů, L. (2018). Review Article: Stress in thin films and coatings: Current status, challenges, and prospects. *Journal of Vacuum Science & Technology*, 36(2). https://doi.org/10.1116/1.5011790

Chapter 3

Discussion

3.1 Introduction:

In this study, we report on how beta-tungsten thin films with different amounts of nitrogen content behave under thermal cycling. We use sputter deposition to create these films, and then subject them to thermal cycling between room temperature and 900 degrees Celsius(°C). The thickness of the films measured by a profilometer was about 200 nanometers, and the texture of the tungsten thin films was analyzed before and after the thermal cycle by using X-ray diffraction. To investigate how nitrogen concentration affects the thin films, two samples were produced, with nitrogen concentrations of 7.27 at.% and 9.49 at.%, respectively. These samples were then heated to 900 °C in a vacuum chamber, while a laser beam was utilized to measure the curvature of the film and determine any changes in the induced thermal stress. In this section, we analyze the results and provide more detailed explanations.

3.2 Converting flow rate to concentration:

The nitrogen content in the thin film was controlled by varying the partial pressure of nitrogen during the deposition. For tungsten thin films, the total number of nitrogen atoms per area of tungsten thin film can be calculated using equation 3.1, where J_{N_2} is the impingement rate of nitrogen, S is the sticking coefficient (0.001) [1], and t the deposition time, 1,000 seconds:

$$N_{N_2} = 2J_{N_2}St \quad (3.1)$$

The ratio of the pressures of nitrogen and argon gases can be found by dividing the flow rate of nitrogen by the flow rate of argon. The individual flow rates of the gases can be found using Eq. 3.2. After establishing the pressure ratio between the nitrogen and argon gases, we deduce that the partial pressure of nitrogen at 1.5 and 2.0 standard cubic centimeters per minute (sccm) is 0.02256 and 0.01687 pascal, respectively, given that the total pressure during the deposition is 3 mTorr, which is 0.4 pascal.

$$J = \frac{3.513 \times 10^{22} \times P}{\sqrt{mT}} \qquad 3.2$$

Next, the impingement rate of nitrogen can be found by substituting the partial pressure of nitrogen into the Knudsen equation (Eq. 3.3), where N_A is Avogadro's number, 6.022×10^{23}, P_{N_2} is the partial pressure of nitrogen, R is the gas constant, 8.314 J/mol/K, T is the temperature, 300 kelvin, and M the molecular weight (28 grams/mol):

$$J_{Nitrogen} = \frac{N_A P_{N_2}}{\sqrt{2\pi MRT}} \qquad 3.3$$

The total number of tungsten atoms per meter square is then calculated using Eq. 3.4:

$$N_w = \frac{\pi h r^2 \rho}{M} \times N_A \qquad 3.4$$

where h is the thickness of the tungsten thin film (200nm), r is the radius of the thin films (0.0508m), ρ is the density of the beta tungsten, 19.12 g/cm^3 [2], and M is the molar mass of tungsten, 183.85 g [3]. Using equation 3.5, we find that the concentrations of nitrogen at 1.5 sccm and 2 sccm are 7.27 at.% and 9.49 at.%, respectively:

$$C = \frac{N_N}{N_N + N_w} \tag{3.5}$$

3.3 Substrate-curvature measurements:

Stresses in tungsten thin films during thermal cycling were measured by using a Frontier Semiconductor 900TC-VAC wafer testing and metrology device located in the Minnesota Nano Center at the University of Minnesota. Throughout the entire experiment, the temperature ramp was set at 10 °C per minute and the substrate curvature was measured every 10 °C as well. During the heating stage, the thermal cycle ramped from 20 °C to 900 °C. After reaching 900 °C, the machine gradually cooled down with a temperature slope of 10 °C .

Before the thermal cycling, a 12-inch silicon light shield was placed around the wafer to prevent interference between the red-orange light coming out of the heat lamps and the red laser light reflected off the wafer. A 750 nm laser was used for stress measurement. During thermal cycling, the stress in the thin films was measured using a substrate-curvature method, and the measured curvature was converted to stress using the Stoney equation (Eq. 3.6).

$$\sigma_f = \frac{Y_s t_s^2}{6t_f}(\frac{1}{R} - \frac{1}{R_0}) \quad 3.6$$

where Y_s is the biaxial modulus of the substrate, R_0 and R are the radii of curvatures of the bare and coated substrates, t_s is the substrate thickness, and t_f is the film thickness. As the film and substrate are thermally cycled together, the difference in thermal expansion between the substrate and the film induces a change in the thin film stress. For purely elastic deformation, this stress change can be represented by equation 3.7 [4]:

$$\Delta\sigma = Y_f \Delta T \Delta\alpha = \left(\frac{E_f(T)}{1 - v_f(T)}\right)(T - T_{RT})\big(\alpha_s(T) - \alpha_f(T)\big) \quad 3.7$$

where $\alpha_s(T)$ and $\alpha_f(T)$ are the thermal expansion coefficient of the substrate and film, $E_f(T)$, $v_f(T)$, Y_f are the temperature-dependent Young modulus, Poisson ratio, and biaxial modulus of the tungsten thin film. Respectively, *T* is the final temperature during the thermal cycle, and T_{RT} is the room temperature.

3.4 Results:

After the deposition process, X-ray diffraction (XRD) is used to examine whether the tungsten thin films are in the beta or alpha phase. The graph represents intensity on the *y*-axis and angle on the *x*-axis. The presence of red and yellow lines in the XRD graph indicate the locations of diffraction, outlining the expected intensity at each point [5]. Figures 3.1 and Figure 3.2 show the XRD results before thermal cycling with both demonstrating characteristics of the beta phase.

Notably, a closer alignment with the blue lines in the (200), (210), and (400) planes suggest the beta phase's presence. Deviations, which experimental results are slightly to the left of the reference lines, observed in the XRD patterns are attributed to the compressive stress of the films after deposition, resulting in a larger lattice plane distance. Due to the Poisson effect, when the thin films experience compressive stress, the lattice spacing in the vertical direction undergoes elongation. According to Bragg's law (equation 3.8), given a constant wavelength, an increase in the interplanar distance ('d') leads to a decrease in angle ('θ'), explaining the observed shift.

$$n\lambda = 2d \times sin\theta \qquad 3.8$$

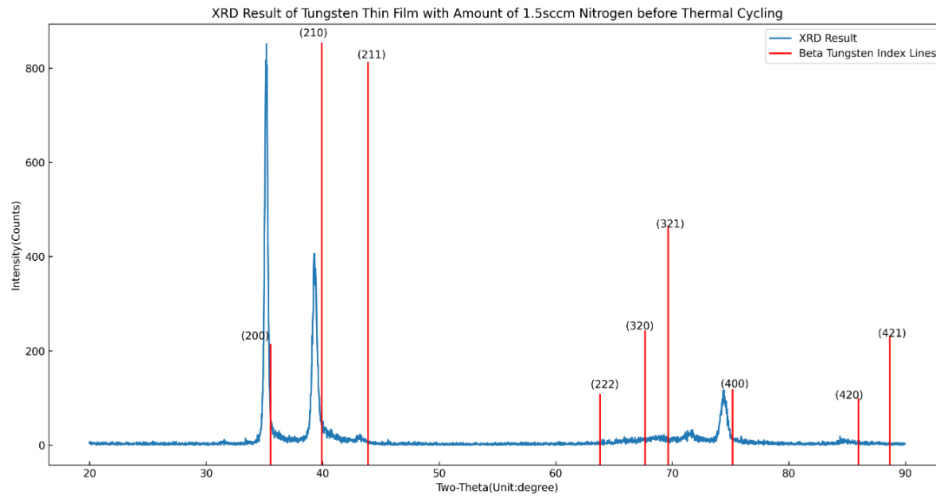

Figure 3.1 XRD result of tungsten thin film with an amount of 1.5 sccm nitrogen before thermal cycling.

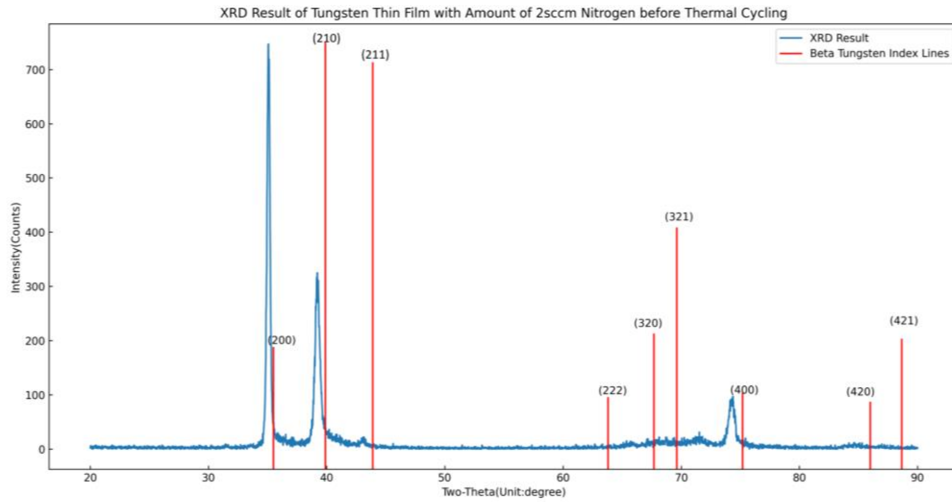

Figure 3.2 XRD result of tungsten thin film with an amount of 2 sccm nitrogen before thermal cycling.

Figures 3.3 and 3.4 are the XRD results after thermal cycling. Almost all of the beta phase has transformed into the alpha phase, and this transformation is evident as the peaks align with those XRD index lines of the alpha phase in the (210), (211), and (220) planes.

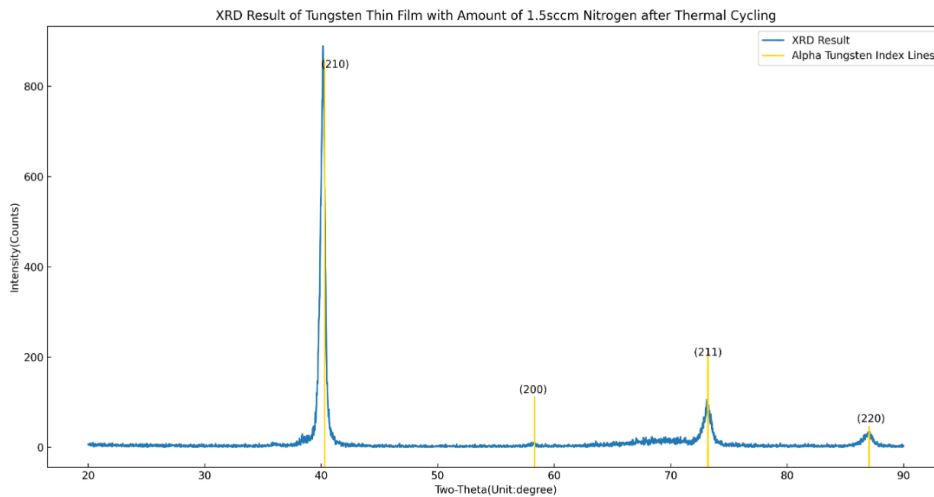

Figure 3.3 XRD result of tungsten thin film with an amount of 1.5 sccm nitrogen after thermal cycling.

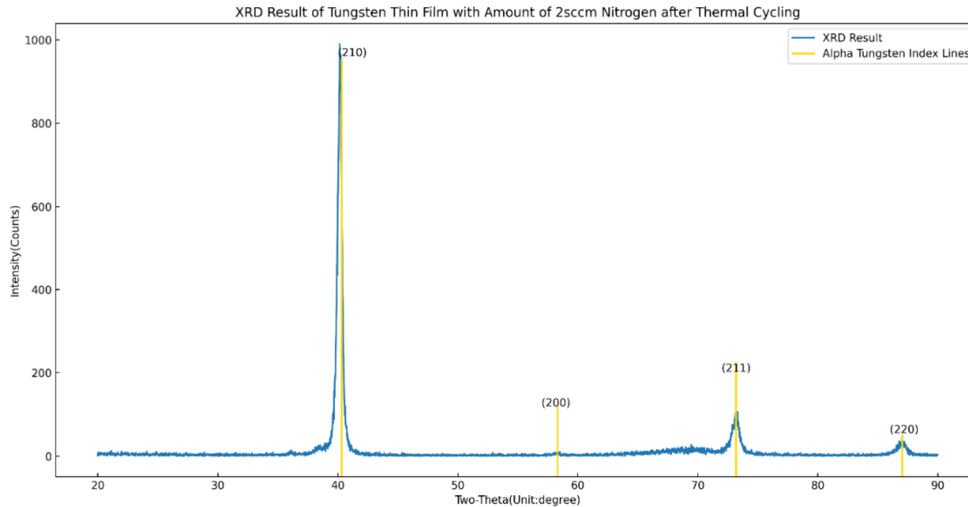

Figure 3.4 XRD result of tungsten thin film with an amount of 2 sccm nitrogen after thermal cycling.

The stress in the films as a function of temperature at the two different nitrogen concentrations is shown in Fig 3.5. The *Y*-axis represents stress, which calculated based on the Stoney equation (Eq. 3.6), and the *X*-axis is the film temperature. In the experiment, the temperature was first raised to 900°C and then allowed to cool back to room temperature.

The provided data delineates the effects of thermal cycling on stress change in the films. Initially, both thin films exhibit small variation in stress. Notably, a significant stress jump happens between 400 and 600 degrees, where stress shifts markedly from about -1700 MPa to -500 MPa. Subsequently, in the range of 600 to 800 degrees, the thin films experience a very small stress change. However, between 800 to 900 degrees, stress notably escalates from -500 to approximately -250 MPa. From 900 to 850 degrees, the stress changes sharply. After 850 degrees, both thin films experience stress changes all the way from 850 to 20 degrees with an almost constant slope.

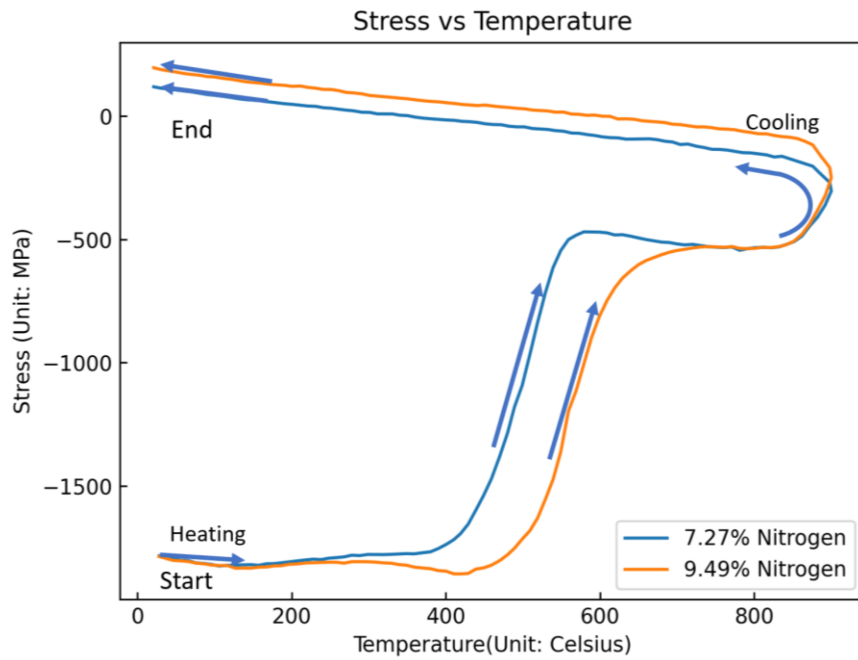

Figure 3.5 Stress change of tungsten thin films with different amounts of nitrogen content during thermal cycling.

3.5 Discussion:

To facilitate better understanding of the stress evolution during the various phases of phase transformation, the entire phase transformation is divided into 6 stages as depicted in Figure 3.6. The first, second, and fourth stages are characterized by small stress variations, while the third and fifth stages are marked by large stress jump. Stage six is identified as the cooling stage. In the rest of discussion, stages 1, 3, 4, 5, and 6 will be explained. At present, the phenomena occurring in stage 2 is uncertain, owing to their inconsistency with our computational findings.

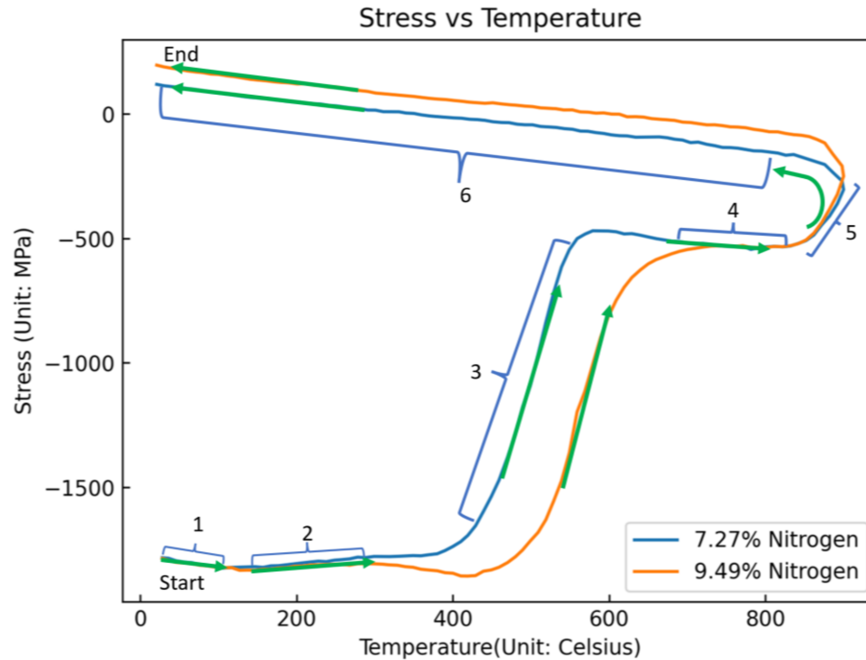

Figure 3.6 Stress change of tungsten thin films with different amounts of nitrogen content during thermal cycling in 6 different stages.

To understand the mechanical properties, Young's Modulus and Poisson's ratio are derived from the temperature-dependent monocrystal elastic constants as shown in equation 3.9-3.12 [6-8]. This study focuses on calculating the effects on the elastic modulus in the [100] direction since [100] direction is normal to the (200) planes, which shows the strongest peak in the XRD result before the thermal cycling. To accurately calculate stress change, we rely on existing data for the temperature-dependent coefficients of thermal expansion for silicon and alpha tungsten from previous research as shown in equation 3.13-3.14 [9-10]. Due to the unavailability of similar data for beta tungsten, our calculations were limited to the use of the coefficient of thermal expansion of alpha tungsten. The strain in the thin films can be determined by integrating the difference of the thermal expansion coefficients between silicon and alpha tungsten(see equation 3.15) [11]. Subsequently, stress with unit of megapascal was deduced by multiplying the strain with the

temperature-dependent biaxial modulus because the stress is acting in both directions as shown in equation 3.16-3.17 [12].

$$C_{11}(T) = (5.2349 \times 10^{12} - 4.5967 \times 10^{8} \times T - 5.467 \times 10^{4} \times T^{2}) \times (10^{-7}) \qquad 3.9$$

$$C_{12}(T) = (2.0445 \times 10^{12} - 0.3403 \times 10^{8} \times T + 3.249 \times 10^{4} \times T^{2}) \times (10^{-7}) \qquad 3.10$$

$$\text{Young's modulus}(E_f(T)) = \frac{(C_{11}(T) - C_{12}(T)) \times (C_{11}(T) + 2 \times C_{12}(T))}{(C_{11}(T) + C_{12}(T))} \qquad 3.11$$

$$\text{Poisson ratio}(\nu_f(T)) = \frac{C_{12}(T)}{C_{11}(T) + C_{12}(T)} \qquad 3.12$$

$$\begin{aligned}\alpha_{Si}(T) = {} & -3.0451 + 0.035705(T + 273.15) - 7.981 \times 10^{-5}(T + 273.15)^{2} \\ & + 9.5783 \times 10^{-8}(T + 273.15)^{3} - 5.8919 \times 10^{-11}(T + 273.15)^{4} \\ & + 1.4614 \times 10^{-14}(T + 273.15)^{5}\end{aligned} \qquad 3.13$$

$$\alpha_{w}(T) = 4.35 \times 10^{-6} + 0.3 \times 10^{-9}T + 0.51 \times 10^{-12}T^{2} \qquad 3.14$$

$$\varepsilon(T) = \int \big(\alpha_{si}(T) - \alpha_{w}(T)\big)dT \qquad 3.15$$

$$Y(T) = \frac{E_f(T)}{1 - \nu_f(T)} \qquad 3.16$$

$$\sigma(T) = Y(T) \times \varepsilon(T) \qquad 3.17$$

Currently, there is limited understanding of stage 1 because of the absence of data on the coefficient of thermal expansion (CTE) for beta tungsten. Given tungsten's melting point of

approximately 3400 degrees Celsius [13], there should be no plastic deformation at room temperature, so it is expected to be elastic. The available information indicates that the behavior is at least consistent with the alpha's coefficient of thermal expansion. As shown in Figures 3.7 and 3.8, the stress in the tungsten thin films closely align with the predicted stress change derived from the alpha tungsten's CTE and temperature-dependent Young's modulus for the initial temperature increase of about 100 degrees Celsius, suggesting that the behavior is predominantly elastic. The reason why the stress went down can be attributed to the increase in temperature, which leads to a subsequent expansion of volume. This expansion of volume causes the thin films to become more compressive, primarily because the coefficient of thermal expansion for tungsten is greater than that of silicon.

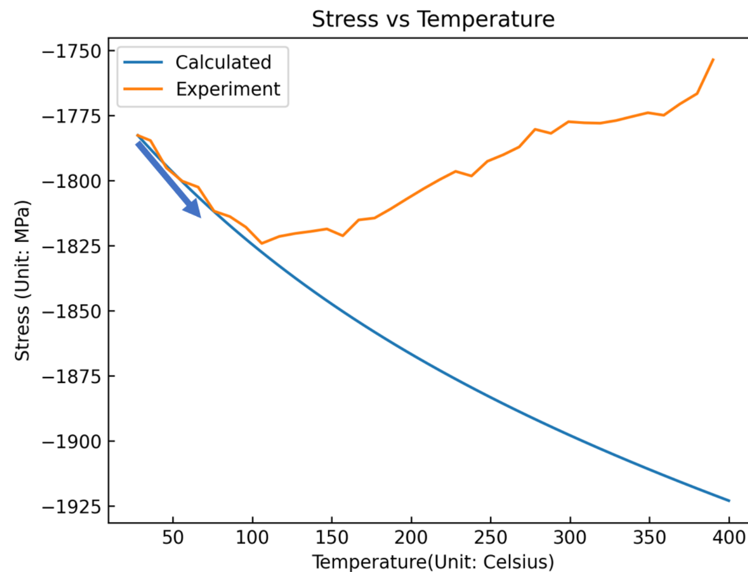

Figure 3.7 Stress of tungsten thin film with 7.27 at.% of nitrogen at a temperature range between 20 degrees and 400 degrees Celsius.

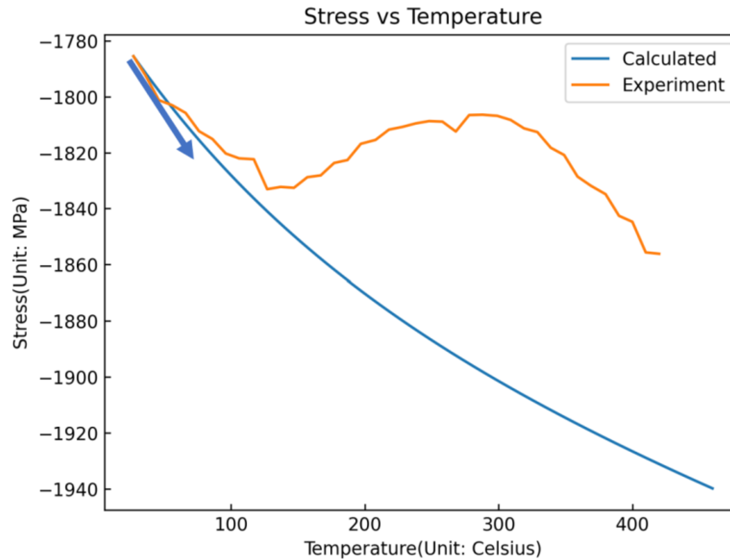

Figure 3.8 Stress of tungsten thin film with 9.49 at.% of nitrogen at a temperature range between 20 degrees and 400 degrees Celsius.

In Stage 4, some discrepancies, are observed in Figures 3.9 and 3.10. The behavior does not precisely align with purely elastic characteristics but is closely akin to it. For thin films containing 7.27 at.% nitrogen, the maximum observed discrepancy between calculated and experimental stress changes is about 35 MPa, and for films with 9.49 at.% nitrogen, it is approximately 15 MPa. When compared to the total phase transformation stress of 1.9 GPa, these variances are relatively minor and may be considered negligible. Consequently, Stage 4 can be regarded as thermally elastic behavior.

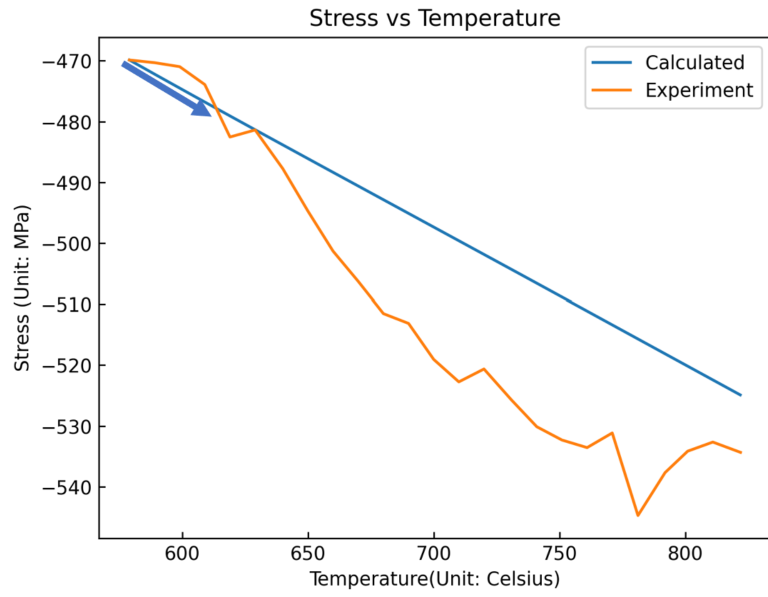

Figure 3.9 Stress of tungsten thin film with 7.27 at.% of nitrogen at a temperature range between 580 and 820 degrees Celsius.

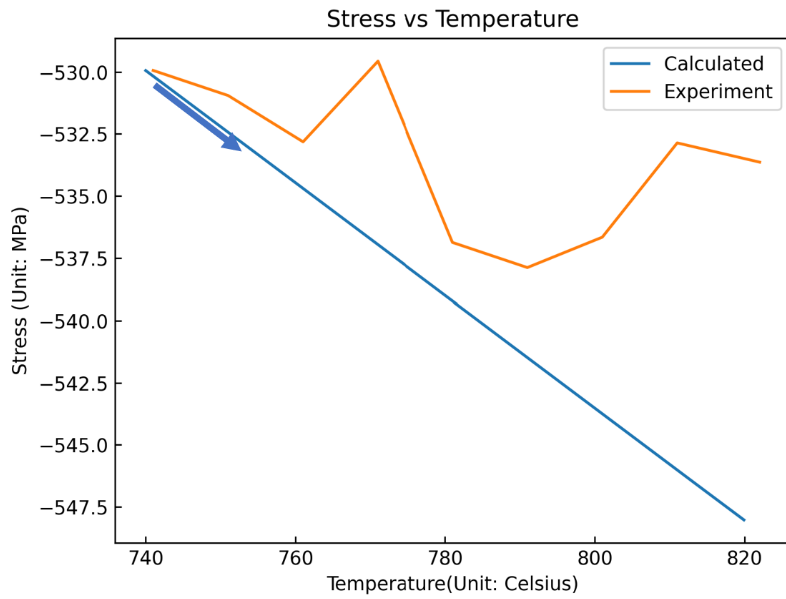

Figure 3.10 Stress of tungsten thin film with 9.49 at.% of nitrogen at a temperature range between 740 and 820 degrees Celsius.

Stage 6, the cooling stage, is depicted in Figure 3.11 and 3.12. Before about 200 degrees Celsius, stress in both thin films closely matched those predication lines from alpha tungsten's coefficient of thermal expansion. While it's unclear whether tungsten is fully transformed into alpha phase between 700 and 200 degrees Celsius, it can be assumed that it is thermally elastic within this range. Post-200 degrees Celsius, deviations between experimental and calculated values are noted. Three potential explanations are posited: First, the experimental results are real, and the results could not be thermal elastic since it does not match the thermal elastic lines. For example, plastic deformation could happen at this range. Secondly, the temperature may be accurate, but the stress calculations could be incorrect. Thirdly, there might be a discrepancy between reported and actual temperatures, suggesting a need for recalibration of the equipment.

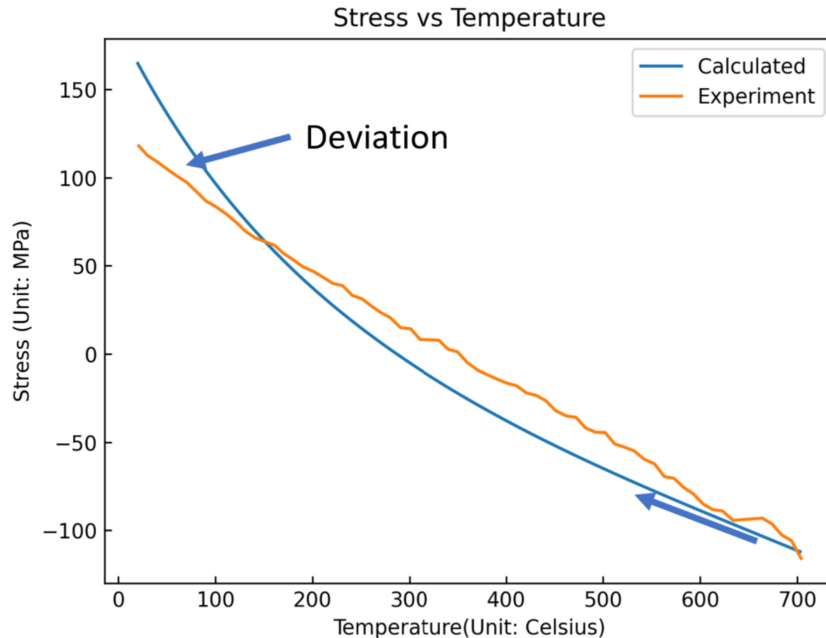

Figure 3.11 Stress of tungsten thin film with 7.27 at.% of nitrogen during the cooling stage at a temperature range between 700 and 20 degrees Celsius.

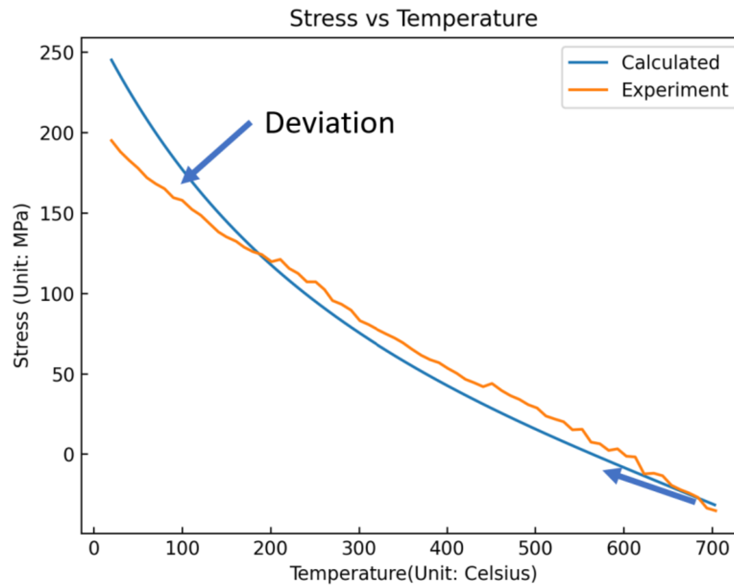

Figure 3.12 Stress of tungsten thin film with 9.49 at.% of nitrogen during the cooling stage at a temperature range between 700 and 20 degrees Celsius.

During Stage 5, a notable stress jump is observed in Figure 3.13. The specific cause of this stress jump remains unverified by current evidence. In Robert Knepper's research, he utilized X-ray Diffraction (XRD) to demonstrate that phase transformation in beta tantalum completes after the first stress jump, evidenced by the diminishing of planes' intensity [14]. While similar experimental data for tungsten is not available, it can be hypothesized that the phase transformation was completed after the first stress jump (stage 3), with the second stress jump potentially attributed to nitrogen leaving the film. Although the exact quantity of nitrogen efflux cannot be directly measured, it can be estimated based on calculations because the total amount of nitrogen in the thin films and stress changes of the second stress jump are known.

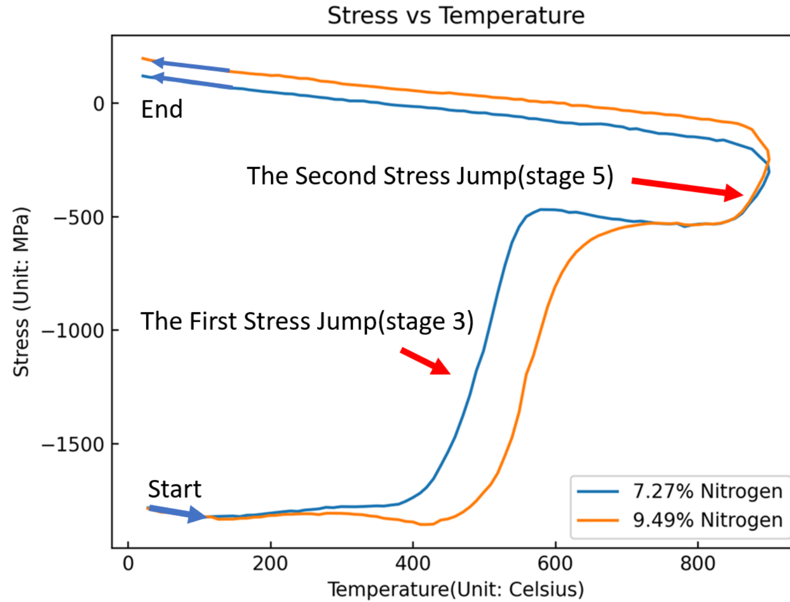

Figure 3.13 Two stress jumps in phase transformation of tungsten thin films.

It is posited that the thin films with higher nitrogen content, such as those with 9.49 at.% compared to 7.27 at.%, would exhibit greater stress jump due to more nitrogen leaving. To estimate the amount of nitrogen released, a linear relationship between dilatation and nitrogen content is assumed. Given the absence of data on nitrogen, calculations are made using oxygen as a proxy because of its similar atomic size and properties. According to Sluiter, the incorporation of one oxygen atom results in an 8.35Å^3 volume increase in tungsten [15]. With a known radius, the total volume of a tungsten thin film is 1.62×10^{-9} cubic meter through calculation in equation 3.18. By dividing the volume of a tungsten thin film, the dilatation of one oxygen atom can be estimated to be 5.56×10^{-21} as shown in equation 3.19 [16]. With known stress change, the total dilatation in the second stress jump can be obtained through equation 3.20 with Young's modulus of 524.3 GPa and Poisson ratio of 0.26

[2,17]. By dividing the dilatation of one oxygen atom (equation 3.21), it is estimated that the tungsten thin films with 7.27 at.% nitrogen released approximately 2.51×10^{17} nitrogen atoms, and the film with 9.49 at.% nitrogen released about 3.05×10^{17} nitrogen atoms.

$$Volume = r^2 \times h \times \pi \qquad 3.18$$

$$e_T = \frac{\Delta V}{V} = \frac{8.35 \times 10^{-30}\ m^3}{1.62 \times 10^{-9}\ \ m^3} = 5.56 \times 10^{-21} \qquad 3.19$$

$$\Delta\sigma = -\frac{E}{(1-\nu)}\frac{e_T}{3} \qquad 3.20$$

$$\text{Number of nitrogen atoms leaving the thin films } = \frac{\text{Total dilatation}}{\text{Dialatation of one oxygen atom}} \qquad 3.21$$

Before the experiment, the change in stress throughout the phase transformation was calculated. The rise in density resulting from the phase transformation causes a change in stress, which can be expressed in equation 3.20. The density of beta-tungsten and alpha-tungsten are 19.12 g/cm^3 and 19.27 g/cm^3 [18], respectively, and a uniform dilatation is expressed in equation 3.22 [17]. In the absence of Poisson's ratio for beta tungsten, the calculations were based on Young's modulus and Poisson's ratio values from alpha tungsten, which are 524.3 GPa and 0.26, respectively [2]. A change in stress of approximately 1.84 GPa in the tensile direction is determined to happen during the transformation from the beta phase to the alpha phase.

After the experiment, the computed result was juxtaposed with the experimental results. Initially, both thin films exhibited a stress level of about 1783 MPa. It was observed that the thin film with a lower nitrogen content displayed lower tensile stresses compared to one with higher nitrogen levels at the end of the experiment. As presented in Figure 3.14, the stress change recorded was 1.9 GPa for a nitrogen content of 7.27 at.% and 1.98 GPa for 9.49 at.% nitrogen. Despite the experimental results exceeding the calculated figures by a margin of 0.06 GPa (equivalent to 60 MPa)—a discrepancy significantly minor relative to the overall stress change of 1.9 GPa—this variance is deemed negligible. Nonetheless, potential reasons for this discrepancy have been posited. First, the accuracy of Young's modulus, Poisson ratio, and density might be in question, potentially containing errors. Secondly, the strain associated with phase transformation may not be purely dilatational.

$$e_T = -\frac{\rho_\alpha - \rho_\beta}{\rho_\alpha} \tag{3.22}$$

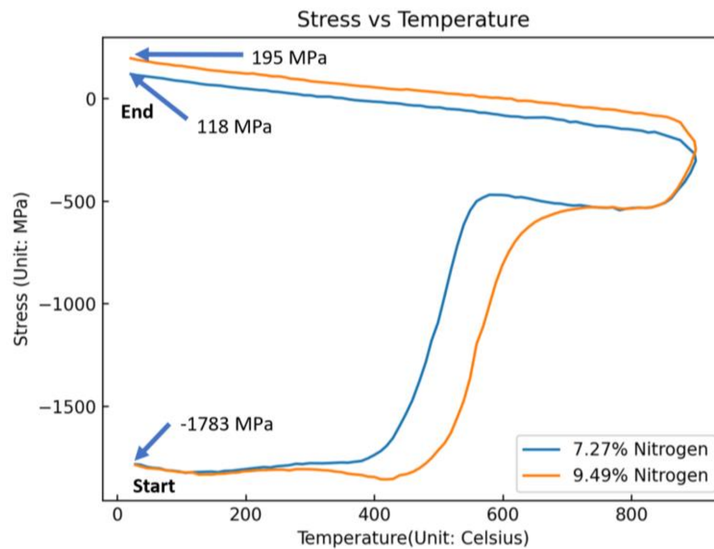

Figure 3.14 Stress in the tungsten thin films at the start and end.

3.6 Conclusion:

The thermomechanical properties of thin films of the metastable beta phase of tungsten have been studied at varying nitrogen partial pressures during sputtering deposition. No evidence of the formation of tungsten nitride was found in the XRD studies, and it is thus concluded that nitrogen affects the tungsten structure by incorporating interstitially into the tungsten thin film. Current evidence does not definitively indicate the precise moment when the tungsten thin films complete the transformation from the beta phase to the alpha phase based on stress measurement results. Hence, our understanding is predominantly inferential, and we draw upon the comparison with calculated stresses to propose that certain stages during the thermal cycling process exhibit thermally elastic characteristics. The data implies that an increased concentration of nitrogen may hinder the phase transition in tungsten films. This is supported by the observation of a greater change in stress in films that contain higher amounts of nitrogen, alongside a delay of stress jump. Moreover, it is recognized that the leaving of nitrogen from thin films contributes, at least in part, to the observed stress change. This is particularly evident given the larger second stress jump in the films with higher nitrogen content.

3.7 References

1. Shen, Y., Mai, Y., McKenzie, D. R., Zhang, Q. C., McFall, W. D., & McBride, W. (2000). Composition, residual stress, and structural properties of thin tungsten nitride films deposited by reactive magnetron sputtering. *Journal of Applied Physics*, *88*(3), 1380–1388. https://doi.org/10.1063/1.373827

2. Nagakubo, A., Lee, H. T., Ogi, H., Moriyama, T., & Ono, T. (2020). Elastic constants of beta tungsten thin films studied by picosecond ultrasonics and density functional theory. *Applied Physics Letters*, *116*(2), 021901. https://doi.org/10.1063/1.5131768

3. Chou, H., Grant, M. P., Bolt, A. M., Guilbert, C., Plourde, D., Mwale, F., & Mann, K. K. (2020). Tungsten increases sex-specific osteoclast differentiation in murine bone. *Toxicological Sciences*. https://doi.org/10.1093/toxsci/kfaa165

4. Abadias, G., Chason, E., Kečkéš, J., Sebastiani, M., Thompson, G. B., Barthel, É., Doll, G. L., Murray, C. E., Stoessel, C. H., & Martinů, L. (2018b). Review Article: Stress in thin films and coatings: Current status, challenges, and prospects. *Journal of Vacuum Science & Technology*, *36*(2). https://doi.org/10.1116/1.5011790

5. Gates-Rector, S., & Blanton, T. N. (2019). The Powder Diffraction File: a quality materials characterization database. *Powder Diffraction*, *34*(4), 352–360. https://doi.org/10.1017/s0885715619000812

6. Lowrie, R., & Gonas, A. M. (1967b). Single-Crystal Elastic Properties of Tungsten from 24° to 1800°C. *Journal of Applied Physics*, *38*(11), 4505–4509. https://doi.org/10.1063/1.1709158

7. Grünwald, E., Nuster, R., Treml, R., Kiener, D., Paltauf, G., & Brunner, R. (2015b). Young's modulus and Poisson's ratio characterization of tungsten thin films via laser ultrasound. *Materials Today: Proceedings*, *2*(8), 4289–4294. https://doi.org/10.1016/j.matpr.2015.09.015

8. Li, W., Kang, L., Fan, K., Zhang, D., & Wang, W. (2018). Temperature and Pressure Dependences of the Elastic Properties of Tantalum Single Crystals Under <100> Tensile Loading: A Molecular Dynamics Study. *Nanoscale Research Letters*, *13*(1). https://doi.org/10.1186/s11671-018-2526-1

9. Watanabe, H., Yamada, N., & Okaji, M. (2004). Linear thermal expansion coefficient of silicon from 293 to 1000 K. *International Journal of Thermophysics*, *25*(1), 221–236. https://doi.org/10.1023/b:ijot.0000022336.83719.43

10. Knibbs, R. H. (1969). The measurement of thermal expansion coefficient of tungsten at elevated temperatures. *Journal of Physics E: Scientific Instruments*, *2*(6), 515–517. https://doi.org/10.1088/0022-3735/2/6/311

11. Murakami, M. (1991). Deformation in thin films by thermal strain. *Journal of Vacuum Science & Technology*, *9*(4), 2469–2476. https://doi.org/10.1116/1.577258

12. Habermehl, S. (2018). Coefficient of thermal expansion and biaxial Young's modulus in Si-rich silicon nitride thin films. *Journal of Vacuum Science & Technology*, *36*(2). https://doi.org/10.1116/1.5020432

13. Wang, L. G., Van De Walle, A., & Alfè, D. (2011b). Melting temperature of tungsten from twoab initioapproaches. *Physical Review B*, *84*(9). https://doi.org/10.1103/physrevb.84.092102

14. Knepper, R., Stevens, B. L., & Baker, S. P. (2006d). Effect of oxygen on the thermomechanical behavior of tantalum thin films during the β–α phase transformation. *Journal of Applied Physics*, *100*(12). https://doi.org/10.1063/1.2388742

15. Sluiter, M. H. F. (2009). Interstitials in tetrahedrally close-packed phases: C, N, O, and F inβ-tungsten from first principles. *Physical Review B*, *80*(22). https://doi.org/10.1103/physrevb.80.220102

16. G'Sell, C., Bai, S., & Hiver, J. (2004). Polypropylene/polyamide 6/polyethylene–octene elastomer blends. Part 2: volume dilatation during plastic deformation under uniaxial tension. *Polymer*, *45*(17), 5785–5792. https://doi.org/10.1016/j.polymer.2004.06.020

17. Knepper, R., Stevens, B., & Baker, S. P. (2006). Effect of oxygen on the thermomechanical behavior of tantalum thin films during the *β*–*α* phase transformation. *Journal of Applied Physics*, *100*(12), 123508. https://doi.org/10.1063/1.2388742

18. Nagakubo, A., Lee, H., Ogi, H., Moriyama, T., & Ono, T. (2020). Elastic constants of beta tungsten thin films studied by picosecond ultrasonics and density functional theory. *Applied Physics Letters*, *116*(2). https://doi.org/10.1063/1.5131768

Chapter 4

Summary and Future Proposed Research

High-purity tungsten thin films with different amounts of nitrogen were deposited, and all the tungsten thin films were thermal cycled to 900 degrees Celsius and experienced approximately 1.9 GPa of stress changes. The experiment result has been compared with our calculation. Part of the stress change during thermal cycling can be assumed to be thermal elastic because it closely matches the calculation. There are two big stress jumps, it can be asserted that part of the stress jump can be contributed by the phase transformation and nitrogen coming out of the films. From the XRD result, it can be concluded that tungsten has been transformed from the beta phase into the alpha phase through thermal cycling, but there is no evidence to know when the transformation was completed. Additionally, the total amount of nitrogen that comes out of the tungsten thin films is not known. However, it can be concluded that thin films with a lower amount of nitrogen experience less stress change during the phase transformation. It can prove that nitrogen has played a role in stabilization for making beta-tungsten.

To gain a more comprehensive understanding of the phase transformation of tungsten, more experiments should be performed. First, the coefficient of thermal expansion of beta tungsten is not known. Without the coefficient of thermal expansion of beta tungsten, we cannot identify whether the beta tungsten has experienced thermal elastic behavior at the beginning. Second, more study needs to be done to find out whether phase transformation is already finished after the first stress jump. If it is confirmed that the phase transformation is finished after the first stress jump, the second stress jump is highly caused by the nitrogen leaving the thin films.

Thirdly, X-ray diffraction should be used for determining the volume fraction of beta tungsten at different temperature stages. In other words, it can precisely tell how beta tungsten changes to the alpha tungsten at which temperature range. Last but not least, resistivity can be used as a reference to measure phase change since beta tungsten has higher resistivity than alpha tungsten.